EUMETSAT
AC SAF
ATMOSPHERIC COMPOSITION MONITORING

AC SAF ORR VALIDATION REPORT

Validated products:

Identifier	Name	Acronym
O3M-317	Offline Total BrO, GOME-2/Metop-C	OTO/BrO

BrO Total VCD April 2019

[molec.cm^{-2}] $\times 10^{13}$
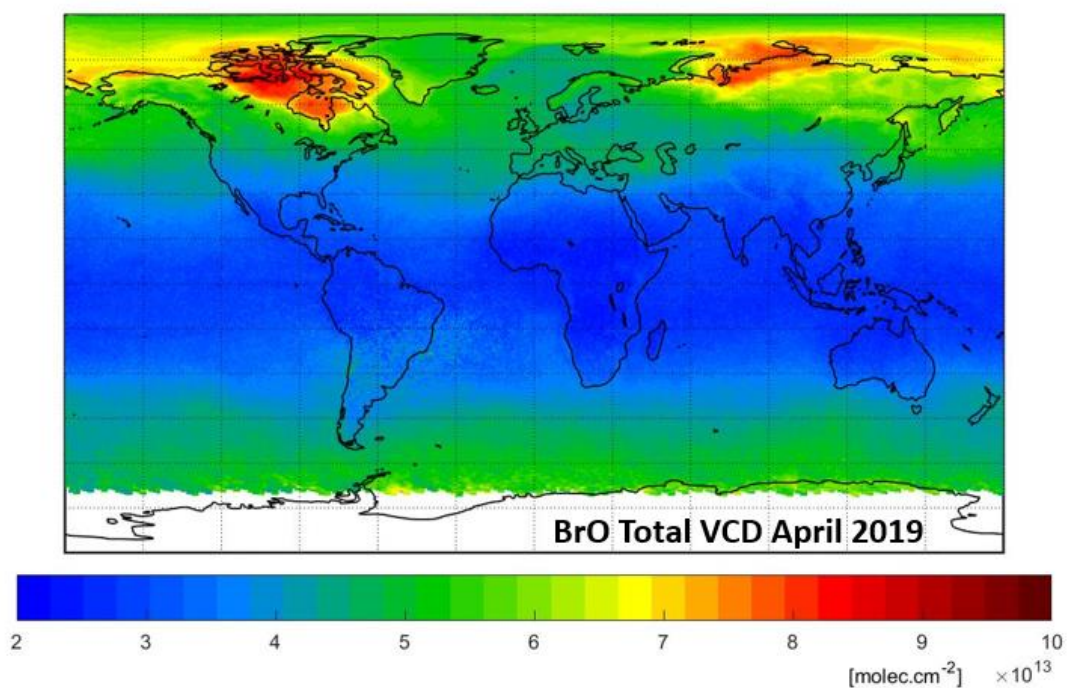
Authors:

Name	Institute
Alexis Merlaud	Belgian Institute for Space Aeronomy
Nicolas Theys	Belgian Institute for Space Aeronomy
François Hendrick	Belgian Institute for Space Aeronomy
Jeroen van Gent	Belgian Institute for Space Aeronomy
Gaia Pinardi	Belgian Institute for Space Aeronomy
Michel Van Roozendael	Belgian Institute for Space Aeronomy
Ka Lok Chan	German Aerospace Center
Klaus Peter Heue	German Aerospace Center
Pieter Valks	German Aerospace Center

Reporting period: February 2019 – July 2019

Input data versions: GOME-2 Level 1B version 6.3

Data processor versions: GDP 4.9, UPAS version 1.4.0

Validation report of GOME-2 GDP 4.9 BrO column data for MetOp-C Operational Readiness Review

CONTENTS

ACRONYMS AND ABBREVIATIONS

AMF	Air Mass Factor, or optical enhancement factor
BAS-NERC	British Antarctic Survey – National Environment Research Council
BIRA	Belgisch Instituut voor Ruimte-Aëronomie
BrO	Bromine monoxide
CAO	Central Aerological Observatory
CNRS/LATMOS	Laboratoire Atmosphère, Milieux, Observations Spatiales du CNRS
DLR	German Aerospace Centre
DMI	Danish Meteorological Institute
DOAS	Differential Optical Absorption Spectroscopy
D-PAF	German Processing and Archiving Facility
Envisat	Environmental Satellite
ERS-2	European Remote Sensing Satellite -2
ESA	European Space Agency
EUMETSAT	European Organisation for the Exploitation of Meteorological Satellites
FMI-ARC	Finnish Meteorological Institute – Arctic Research Centre
GAW	WMO's Global Atmospheric Watch programme
GDOAS/SDOAS	GOME/SCIAMACHY WinDOAS prototype processor
GDP	GOME Data Processor
GOME	Global Ozone Monitoring Experiment
GVC	Ghost Vertical Column
H_2O	water vapour
IASB	Institut d'Aéronomie Spatiale de Belgique
IFE/IUP	Institut für Fernerkundung/Institut für Umweltphysik
IMF	Remote Sensing Technology Institute
INTA	Instituto Nacional de Técnica Aeroespacial
KSNU	Kyrgyzstan State National University
LOS	Line Of Sight
MIPAS	Michelson Interferometer for Passive Atmospheric Sounding
NDACC	Network for the Detection of Atmospheric Composition Change
NDSC	Network for the Detection of Stratospheric Change
NIWA	National Institute for Water and Atmospheric research
BRO	nitrogen dioxide
O_3	ozone
O3M-SAF	Ozone and Atmospheric Chemistry Monitoring Satellite Application Facility
OCRA	Optical Cloud Recognition Algorithm
OMI	Ozone Monitoring Instrument
ROCINN	Retrieval of Cloud Information using Neural Networks
RRS	Rotational Raman Scattering
RTS	RT Solutions Inc.
SAOZ	Système d'Analyse par Observation Zénithale
SCD	Slant Column Density
SCIAMACHY	Scanning Imaging Absorption spectroMeter for Atmospheric CHartography
SNR	Signal to Noise Ratio
SZA	Solar Zenith Angle
TEMIS	Tropospheric Emission Monitoring Internet Service
UNESP	Universidade Estadual Paulista
UPAS	Universal Processor for UV/VIS Atmospheric Spectrometers
UVVIS	ground-based DOAS ultraviolet-visible spectrometer
VCD	Vertical Column Density
WMO	World Meteorological Organization

Introduction to EUMETSAT Satellite Application Facility on Atmospheric Composition monitoring (AC SAF)

Background

The monitoring of atmospheric chemistry is essential due to several human caused changes in the atmosphere, like global warming, loss of stratospheric ozone, increasing UV radiation, and pollution. Furthermore, the monitoring is used to react to the threats caused by the natural hazards as well as follow the effects of the international protocols.

Therefore, monitoring the chemical composition and radiation of the atmosphere is a very important duty for EUMETSAT and the target is to provide information for policy makers, scientists and general public.

Objectives

The main objectives of the AC SAF is to process, archive, validate and disseminate atmospheric composition products (O_3, NO_2, SO_2, BrO, HCHO, H_2O, OClO, CO, NH3), aerosol products and surface ultraviolet radiation products utilising the satellites of EUMETSAT. The majority of the AC SAF products are based on data from the GOME-2 and IASI instruments onboard Metop satellites.

Another important task besides the near real-time (NRT) and offline data dissemination is the provision of long-term, high-quality atmospheric composition products resulting from reprocessing activities.

Product categories, timeliness and dissemination

NRT products are available in less than three hours after measurement. These products are disseminated via EUMETCast, WMO GTS or internet.

- Near real-time trace gas columns (total and tropospheric O_3 and NO_2, total SO_2, total HCHO, CO) and high-resolution ozone profiles
- Near real-time absorbing aerosol indexes from main science channels and polarization measurement detectors
- Near real-time UV indexes, clear-sky and cloud-corrected

Offline products are available within two weeks after measurement and disseminated via dedicated web services at EUMETSAT and AC SAF.

- Offline trace gas columns (total and tropospheric O_3 and NO_2, total SO_2, total BrO, total HCHO, total H_2O) and high-resolution ozone profiles
- Offline absorbing aerosol indexes from main science channels and polarization measurement detectors
- Offline surface UV, daily doses and daily maximum values with several weighting functions

Data records are available after reprocessing activities from the EUMETSAT Data Centre and/or the AC SAF archives.

- Data records generated in reprocessing
- Lambertian-equivalent reflectivity
- Total OClO

Users can access the AC SAF offline products and data records (free of charge) by registering at the AC SAF web site.

More information about the AC SAF project, products and services: https://acsaf.org/
AC SAF Helpdesk: helpdesk@acsaf.org
Twitter: https://twitter.com/Atmospheric_SAF

DATA DISCLAIMER FOR THE METOP-B GOME-2 TOTAL BRO (NTO/OTO) DATA PRODUCTS

In the framework of EUMETSAT's Satellite Application Facility on Atmospheric Composition Monitoring (AC-SAF), GOME-2 bromine oxide (BrO) total column data products, as well as associated cloud parameters, are delivered operationally off-line. Those data products are generated at DLR from MetOp-C GOME-2 measurements using the UPAS environment version 1.4.0, the level-0-to-1 v6.3 processor and the level-1-to-2 GDP v4.9 DOAS retrieval processor (see TN-DLR-ATBD 2013 and TN-DLR-PUM 2013). BIRA-IASB ensures detailed quality assessment of algorithm upgrades and continuous monitoring of GOME-2 BrO data quality with a recurring geophysical validation using correlative measurements from the NDACC ground-based network and from other satellites, modelling support, and independent retrievals.

This present the initial validation of MetOp-C GOME-2 BrO column data recorded over February 2019 through July 2019. Total BrO column data are compared to similar Envisat SCIAMACHY, MetOp-A, and MetOp-B GOME-2 results, and to ground-based columns retrieved from Zenith-Sky measurements at the Harestua station.

The main results are summarized hereafter:

- The current quality of the MetOp-C GOME-2 radiance and irradiance spectra (level-1b data version 6.3) in the 332-359 nm spectral window enables stable DOAS retrievals

- Despite a small positive bias in the northern stations, the Metop-C GOME-2 total BrO VCDs are consistent with GOME-2B and ground-based observations at Harestua, Norway. On average, the optimal accuracy of 15% is reached.

- The Southern Atlantic Anomaly is less degrading the Metop-C BrO VCDs products than it is for the Metop-B products

A. INTRODUCTION

A.1. Scope of this document

The present document reports on the verification and validation of MetOp-C GOME-2 BrO total column data over the Feb. 2019 – Jul. 2019 time period, produced by the GOME Data Processor (GDP) version 4.9 operated at DLR on behalf of EUMETSAT. This report includes verification work performed using the BIRA-IASB scientific retrieval tool synchronized on the GDP settings, as well as comparisons with SCIAMACHY, GOME-2A, GOME-2B and ground-based measurements. The aim is to investigate the consistency of the GOME-2C BrO total columns and whether the GOME-CB BrO product fulfill the user requirements in terms of accuracy (Threshold accuracy: 50%; Target accuracy: 30%; Optimal: 15%), as stated in the ACSAF Service Specification Document (https://acsaf.org/docs/AC_SAF_Service_Specification.pdf).

A.2. Preliminary remarks

BrO total columns as generated from GDP version 4.9 for GOME-2C represent a new GOME-2 product, generated within the GDP operational environment system at DLR.

The aim of the present document is first to report on the status of the verification of the MetOp-C GOME-2 BrO column against a synchronized scientific algorithm available at BIRA. For this exercise, BrO retrieval settings selected by DLR scientists for GDP version 4.9 are being used. The consistency of this BrO product is then explored by performing various comparisons with existing correlative data sets, including scientific data sets from SCIAMACHY, GOME-2A, and GOME-2B. Ground-based BrO column measurements available for the stations at Harestua in Norway are also used in an attempt to further document the geophysical consistency of the GOME-2 BrO product.

The validation studies presented in this document were carried out at the Belgian Institute for Space Aeronomy (IASB-BIRA, Brussels, Belgium) and at DLR Remote Sensing Technology Institute (DLR-IMF, Oberpfaffenhofen, Germany) in the framework of EUMETSAT Satellite Application Facility on Atmospheric Composition Monitoring (AC-SAF).

A.3. Plan of this document

This document is divided in four main parts, addressing respectively the description of the retrieval settings applied for the BrO product, the verification of this product, comparisons against satellite data and comparisons against ground-based measurements at Harestua. This is followed by concluding remarks and perspectives for future work.

B. GOME-2 BRO COLUMN RETRIEVAL AND VALIDATION DATASETS

B.1. Total BrO columns retrieval

The detailed DOAS settings used for GOME-2 BrO slant columns retrieval are given in Table B.1.

Fitting interval	332 – 359 nm
Sun reference	Sun irradiance from file
Wavelength calibration	Wavelength calibration of sun reference optimized by NLLS adjustment on convolved Chance and Spurr solar lines atlas
Absorption cross-sections	
- BrO	Fleischmann et al., 223°K
- NO$_2$	GOME FM3, 243°K
- Ozone	Brion et al. 1998, convolved at GOME-2 resolution, 218°K + 243°K Two pseudo-cross-sections accounting for non-linearity of O3absorption (Pukite et al., 2010)
- H$_2$CO	Meller et al. 2000 at 297K
- OClO	Bogumil et al., 2003 at 293K
- Ring effect	2 Ring eigenvectors generated using SCIATRAN
- Polarization	GOME-2 FM-203 Calibration Key Data, Eta and Zeta
Polynomial	5rd order (6 parameters)
Intensity offset correction	Constant +slope

Table B.1. DOAS settings used for GOME-2 BrO slant column verification

The retrieved BrO slant columns are converted into vertical columns through air mass factors (AMF), which are calculated for each pixel. These AMFs are generated with the LIDORT 3.3 radiative transfer model in the GDP 4.9 environment, using pure stratospheric BrO profiles.

B.2. Validation data sets

We have used the following datasets for the validation of the Metop-C BrO total VCDs:

- GOME-2B total BrO VCDs (GDP 4.8), which are already validated and found to be within the target accuracy (30%) and even within the optimal accuracy (15%) if the tropospheric content is considered in the comparison with ground-based data

- Ground–based total BrO columns at Harestua, Norway (Hendrick et al., 2007, 2008, 2009). BIRA-IASB is operating ground-based DOAS systems (Beijing, Jungfraujoch, Observatoire de Haute-Provence)

In addition, we show two other BrO datasets in this report:

- GOME-2A is operating in parallel to GOME-2B and C. However, GOME-2A suffers for many years of a strong instrumental degradation affecting the quality of the total BrO column product.

- SCIAMACHY total BrO columns proved to be of very good quality even a decade long after launch but unfortunately the data record ends on the 8th of April 2012. SCIAMACHY cannot be used properly to validate GOME-2B total BrO columns. Nevertheless, for the purpose of this study, we have averaged 4 years of SCIAMACHY data (2007-2010) to investigate whether the observed latitudinal-time variations of GOME-2C BrO total columns were geophysically coherent or not.

C. VERIFICATION OF SLANT COLUMNS

C.1 QDOAS versus UPAS retrievals

To verify the BrO slant columns, the retrieval software of BIRA-IASB was synchronised with the GDP 4.9 processor, using a common set of slant column retrieval settings, as documented in Table B.1. Comparisons between the two processing systems were performed on a limited set of GOME-2 orbits. Results of these comparisons are illustrated in Figure C.1 for 6 February 2019. As can be seen, a good level of agreement was obtained, demonstrating the consistency between the two slant column fitting algorithms.
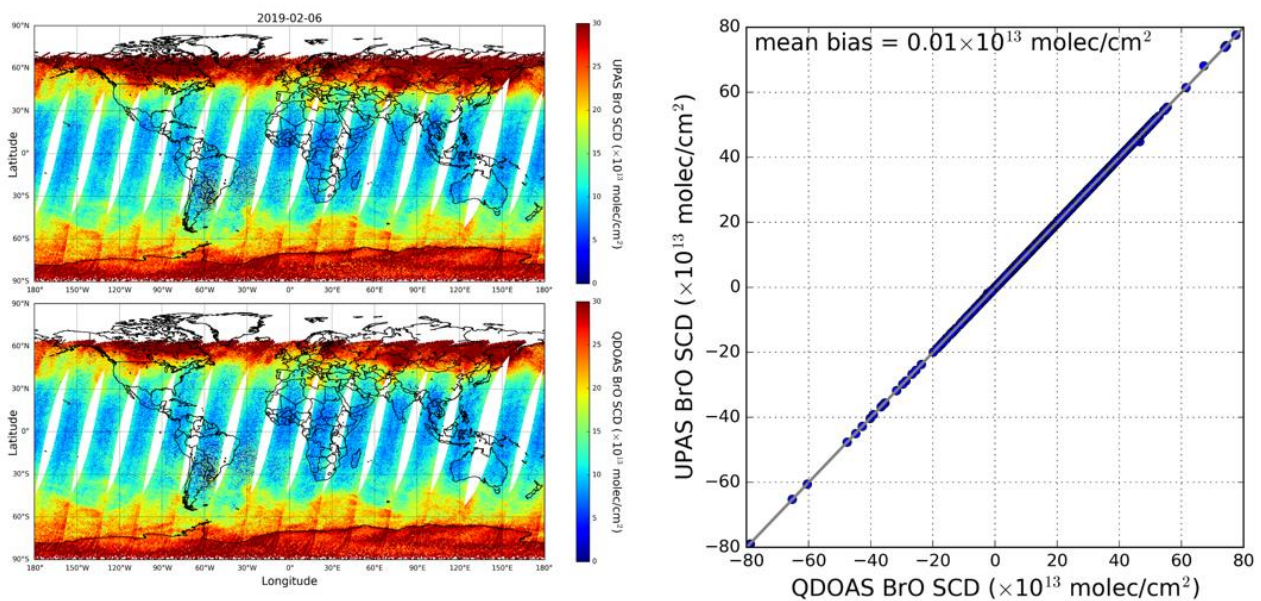
Figure C.1: Comparison of Metop-C BrO slant columns retrieved with GDP 4.9 and with the BIRA-IASB scientific algorithm. DOAS settings were synchronized according to Table 1.

C.2 Consistency with previous GOME-2 instruments

We further investigated the consistency of the GOME2-C BrO slant columns comparing two sets of close orbits of MetOp-A, MetOp-B, and MetOp-C on 15 April 2019, as shown in Figure C.2.

This comparison indicates a good agreement between GOME2-B and GOME2-C outside the South Atlantic Anomaly (SAA), which strongly degrades the fit residual above this area. The noise on GOME2-B is higher than on GOME2-C but the overall pattern of the BrO slant columns along the orbit are similar for the two instruments. The comparison with GOME-2A is not as good due to the aforementioned instrumental degradation.
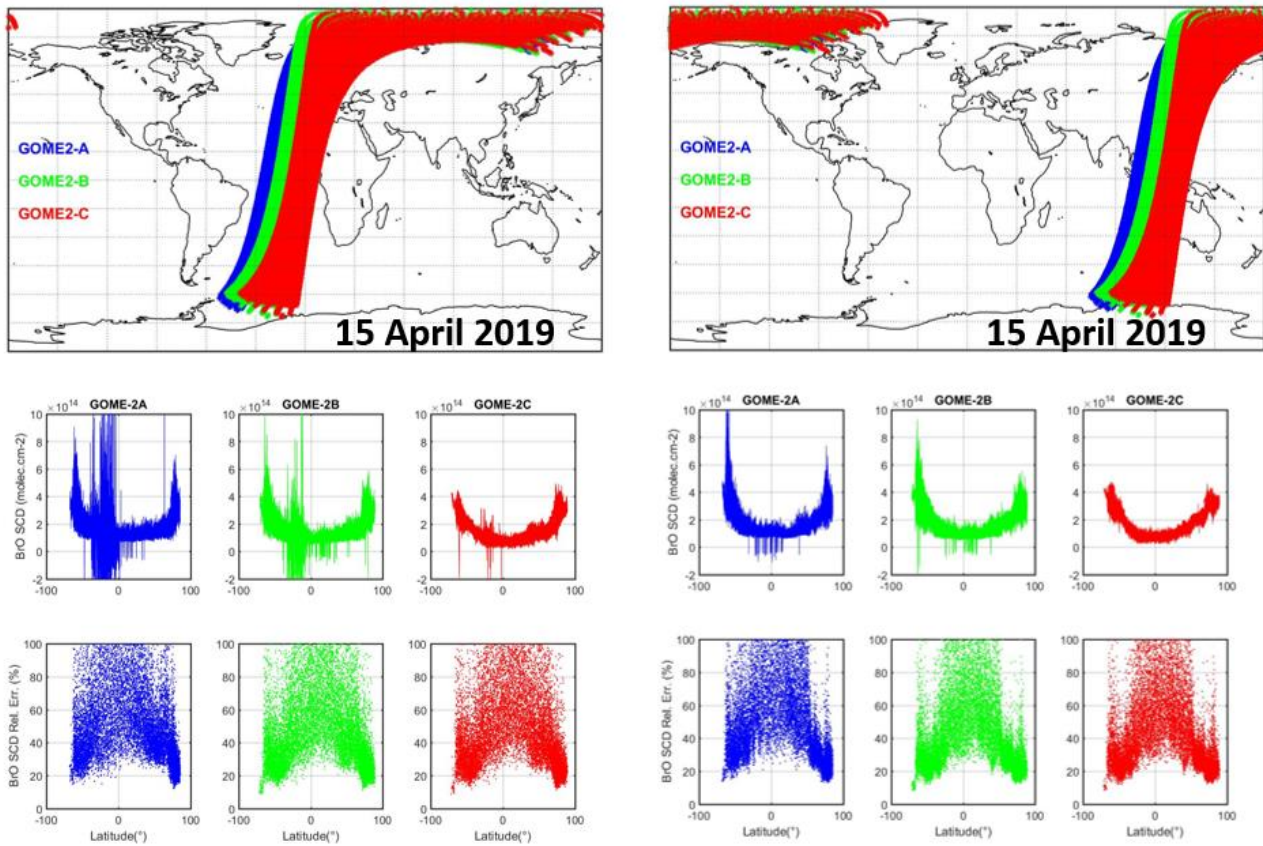
Figure C.2: Comparison of Metop-C (using GDP 4.9) BrO slant columns with similar product Metop-A (GDP 4.8) and Metop-B (GDP 4.8) for two sets of close orbits on 15 April 2019

C.3 Cross-talk with H₂CO

The ORR report for the GOME-2C H_2CO product (SAF/AC/IASB/VR/HCHO) pointed out a dependence on the viewing angle, with higher H_2CO SCDs in nadir and lower values at off-nadir scan angle). This pattern is not visible in Metop-B data (see Fig C.1.2. of the H_2CO report).

Considering the spectral interference between BrO and H_2CO (Pinardi et al., 2013), we looked for such an angular dependence in the BrO SCD products.

	REFERENCE:	**SAF/AC/IASB/VR/BRO**
	ISSUE:	1/1
	DATE:	19 May 2020
	PAGES:	Page **12** of **27**

EUMETSAT
AC SAF
ATMOSPHERIC COMPOSITION
MONITORING
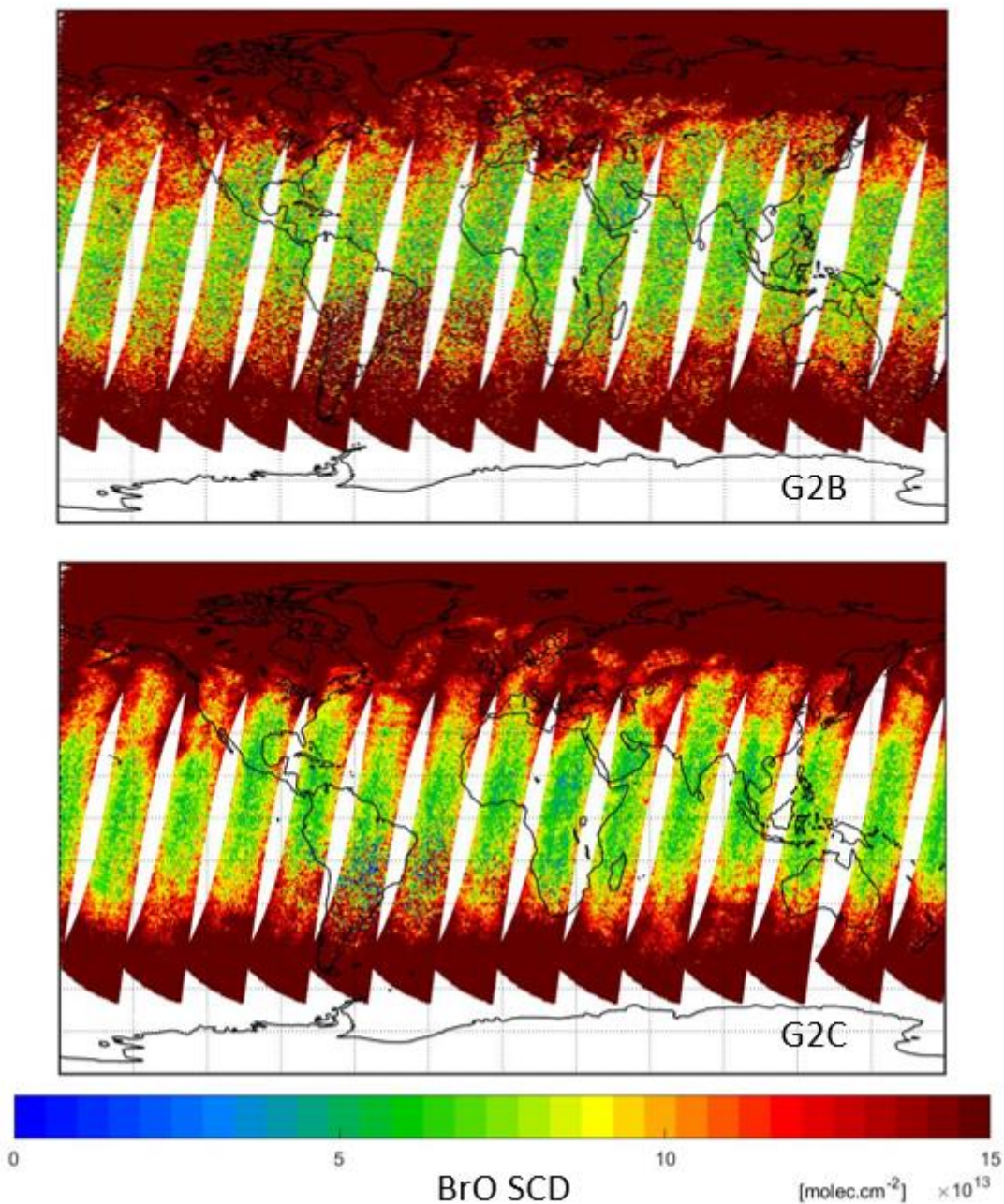
Figure C.3 Metop-B (upper panel) and Metop-C (lower panel) BrO slant columns on 15 April 2019. Compared to Fig C.1, we have reduced the dynamic range of the color bar to emphasize the East-West dependency in G2C.

Figure C3 shows maps of GOME-2B and GOME-2C BrO SCDs for 15 April 2019, with a saturated color scale to enhance the small variations on the low end of the dynamic range. For GOME-2C only, it appears that the BrO SCDs systematically increase on the sides of the swath, with smaller BrO SCDs for viewing angles close to nadir, which is consistent with the expected cross-talk between BrO and H_2CO.
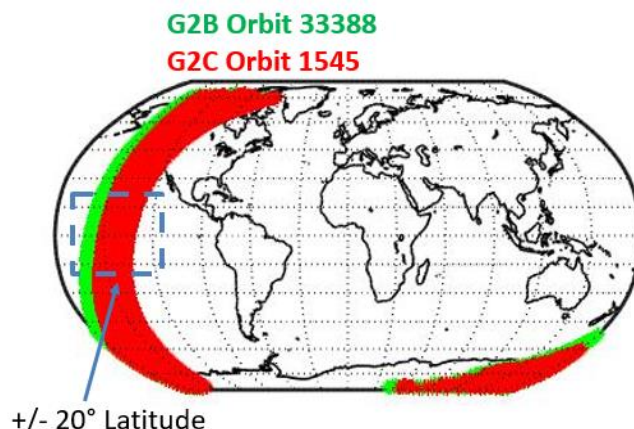
Figure C.4 Footprints of the Metop-B and Metop-C orbits of 23 Febuary 2019 which we further analysed on Fig. C.5, Fig C.6, Fig D.8, focusing on the area within the dashed line square.

We further investigated the cross talk between BrO and H_2CO by studying more quantitatively a reference area above the equatorial Pacific, as seen by GOME-2B and GOME-2C on a given date (23 February 2019). Figure C.4 shows the selected orbits and the reference area.

Figure C.5 shows the SCDs of H_2CO and BrO for Metop-B and Metop-C on 23 February 2019 above the reference area, as a function of the pixel number in the forward scan. The pixel number is linked with the viewing angle, with pixels 0 to 23 corresponding to the forward scan and pixels 24 to 31 corresponding to the backward scan. For GOME-2B, the BrO and H_2CO SCDs only show limited if any angular dependence on the pixel number, but such a dependence clearly appears in GOME-2C, confirming Fig C.3, which corresponds to another day.

Figure C.6 shows the same data as Figure C.5, but only for GOME-2C and including the backscan pixels, the figure further illustrates the cross talk between BrO and H_2CO. Regarding the GOME-2C BrO SCDs, the enhancement of the SCDs on the sides of the swath compared to the minimum (at pixel 15) is up to around 80% (pixel 0) and 50% (pixel 24). Note that a part of this observed bias (30%) is expected due to the AMF dependency on the Viewing zenith angle (1/cos(VZA)). The minimum BrO SCD of pixel 15 seems to be representative for a realistic SCD baseline when compared to GOME-2B, which does not exhibit such an angular dependence. This is consistent with the GOME-2 SCDs extracted above Harestua, which are shown in Figure C.7, where GOME-2C appears slightly high biased compared to GOME-2B and GOME-2A. In the next section, we investigate this effect in the corresponding BrO VCDs (Fig. D.8).
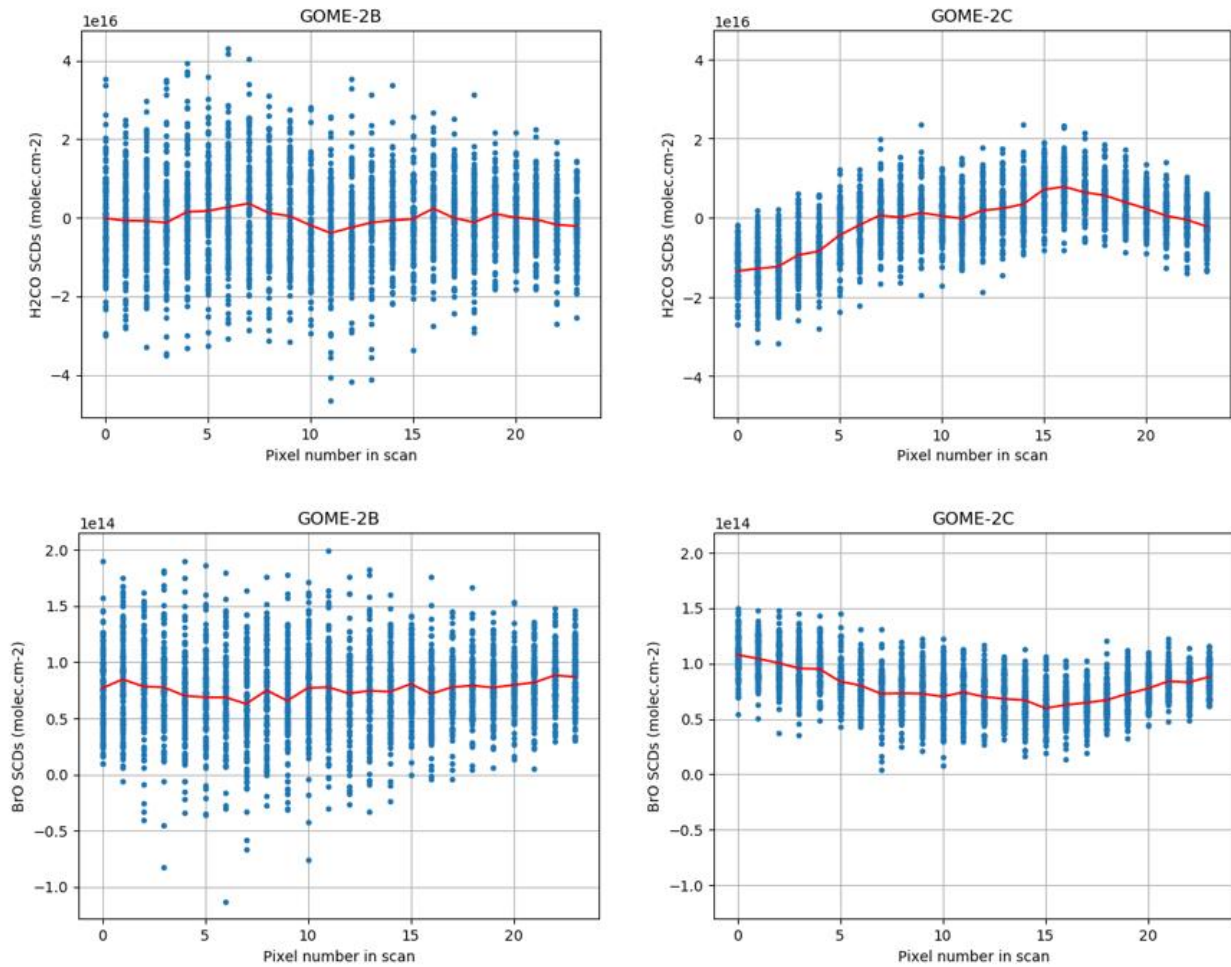
Figure C.5 Metop-B and Metop-C H₂CO and BrO SCDs versus pixel number in the scan for the forward scans of the orbits and area of Fig. C.4. For each graph, the red line shows the average of the pixels in a given scanning position.
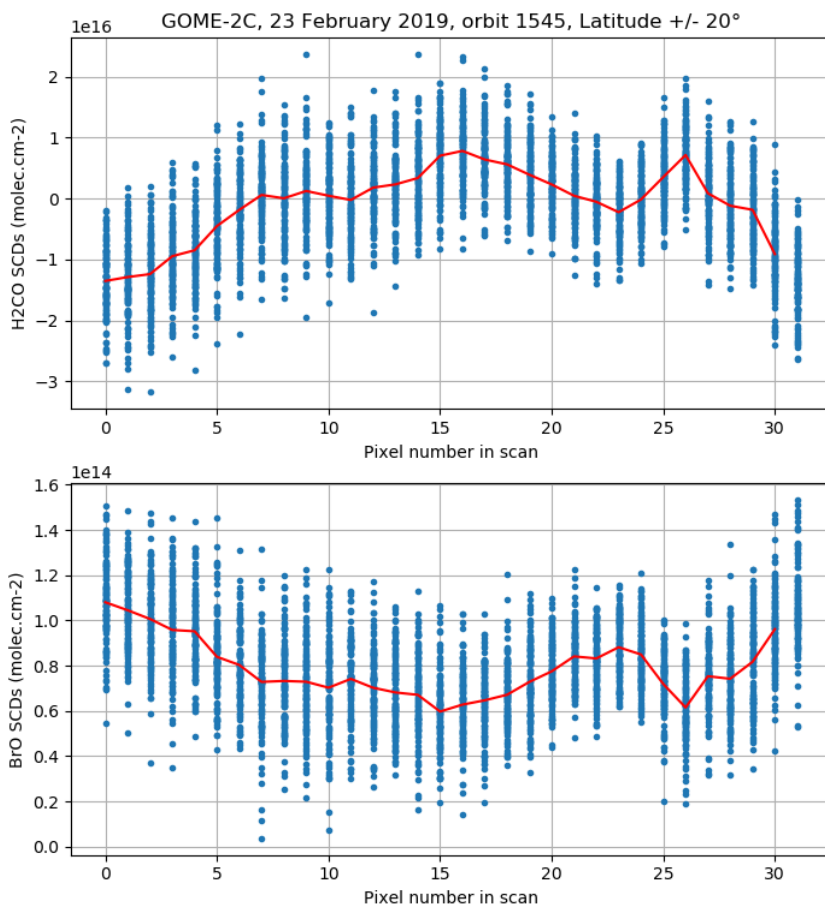
Figure C.6 Metop-C H₂CO and BrO SCDs versus pixel number in the scan (pixels 24 to 31 correspond to the backward scan). For each graph, the red line shows the average of the pixels in a given scanning position.
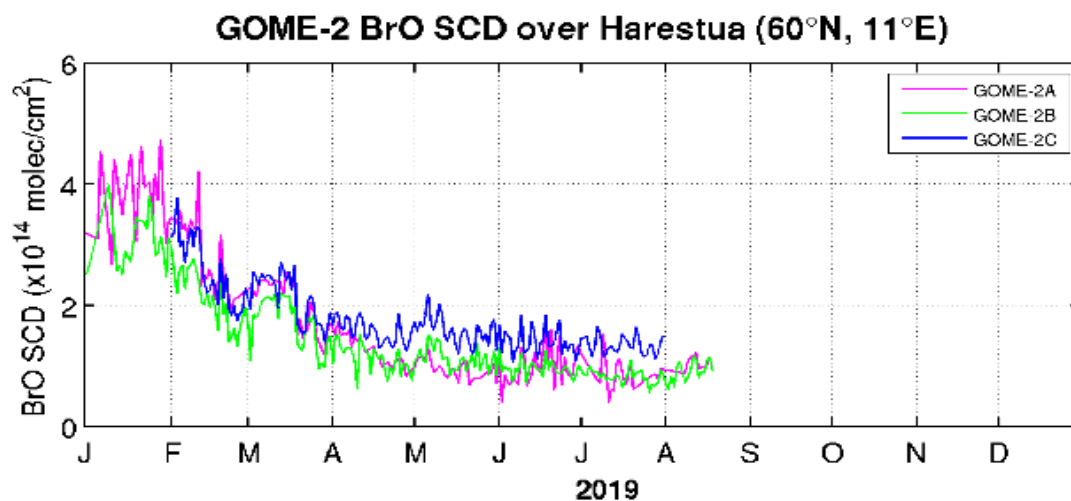
Figure C.7. Time series of the BrO SCDs measured by the three GOME-2 instruments above Harestua for January to August 2019.

D. EVALUATION OF THE BRO COLUMN DATA PRODUCT

D.1 Internal consistency

We first check the internal consistency of the GOME-2C BrO data, aiming to evaluate if the overall total column patterns are as expected. Figure D.1 shows the monthly averaged GOME2-C BrO VCDs for the 6 investigated months. GOME-2C clearly shows the enhanced BrO in the polar regions associated to the well know tropospheric BrO explosions phenomenon. Moreover, large scale patterns extending to the mid-latitudes and associated to stratospheric BrO (Theys et al., 2009, 2011) are also visible.
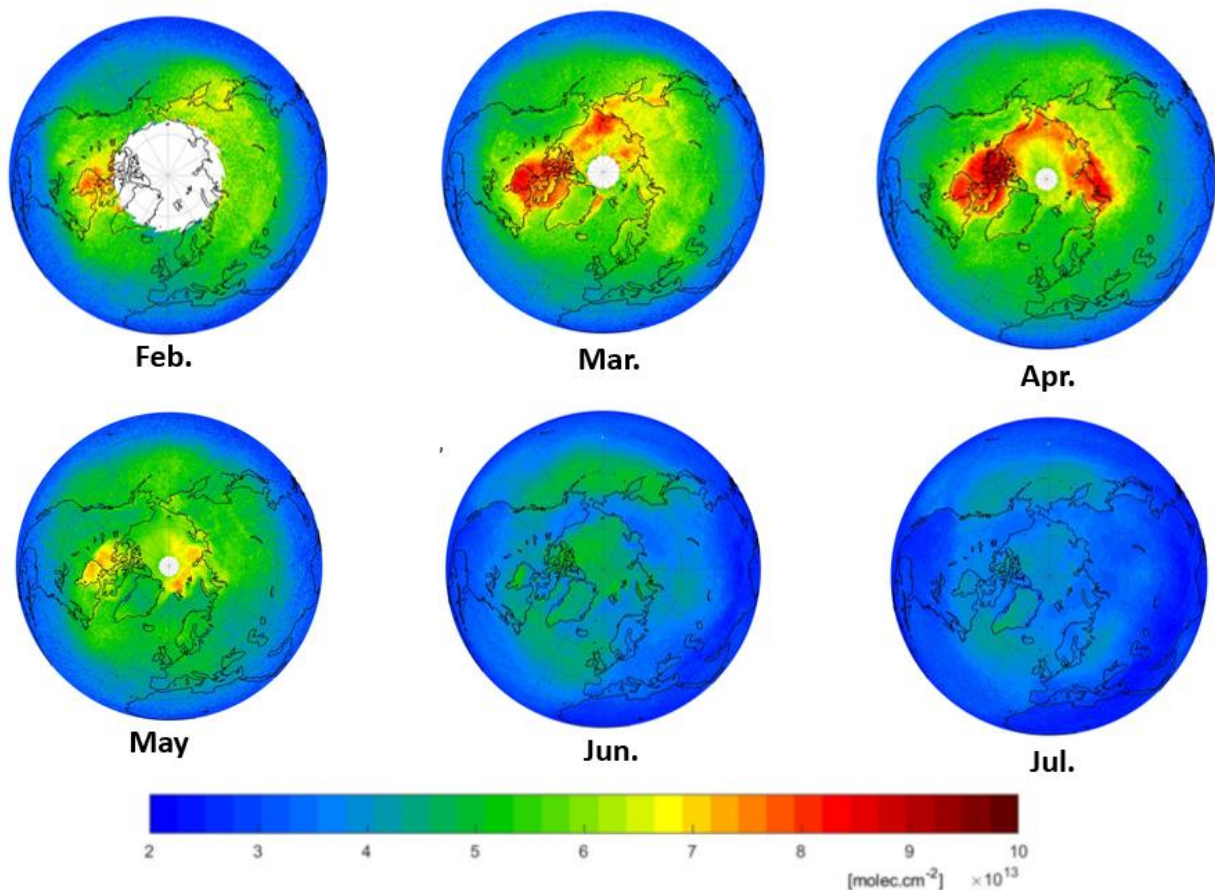
Figure D.1 Monthly averaged BrO vertical columns derived from GOME-2C in the Northern hemisphere for February to July 2019.

D.2 Comparison against satellite data

In a second step, we qualitatively compare the BrO column results obtained from GOME-2B and GOME-2C for one particular month, i.e. April 2019. Figure D.2 presents the two associated world maps. We observe a remarkable agreement between GOME-2B and GOME-2C BrO columns. The only area where the two

dataset clearly disagree is the SAA, which clearly affects GOME2-B but barely seems to degrade the quality of the GOME-2C BrO VCDs.
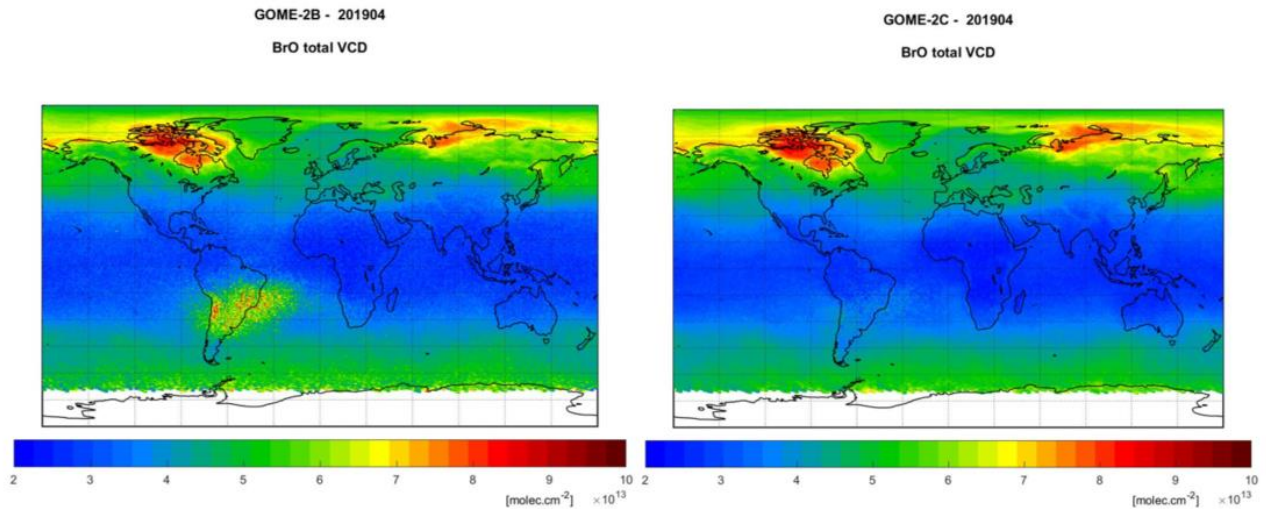
Figure D.2: Comparison of the BrO total VCDs from Metop-B (left panel) and Metop-C (right panel) for April 2019.

Figure D.3 further illustrates the good geophysical consistency of the total BrO column products from the three different GOME-2 instruments when averaged for April 2019. We observe similar BrO column spatial patterns, with somewhat higher GOME-2A BrO VCDs compared to the two other sensors, as can be expected from the higher slant GOME-2A slant columns (Figure C.2). It is probably due to the smaller swath of GOME2-A (the SCDs are divided by smaller AMFs).
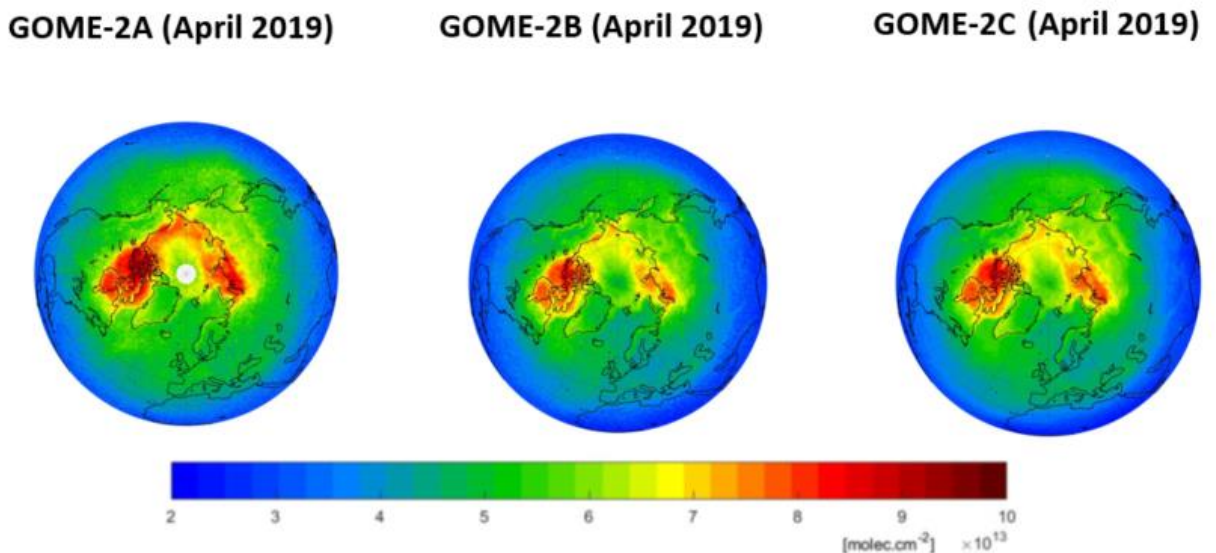
Figure D.3 Monthly averages of total BrO vertical columns in Arctic spring (April 2019) from the three GOME2 instruments.

We now compare the different satellite datasets quantitatively. We analyze the differences between GOME-2C, GOME-2B, and the SCIAMACHY climatology for 12 overpass files sites shown in Figure D.4.
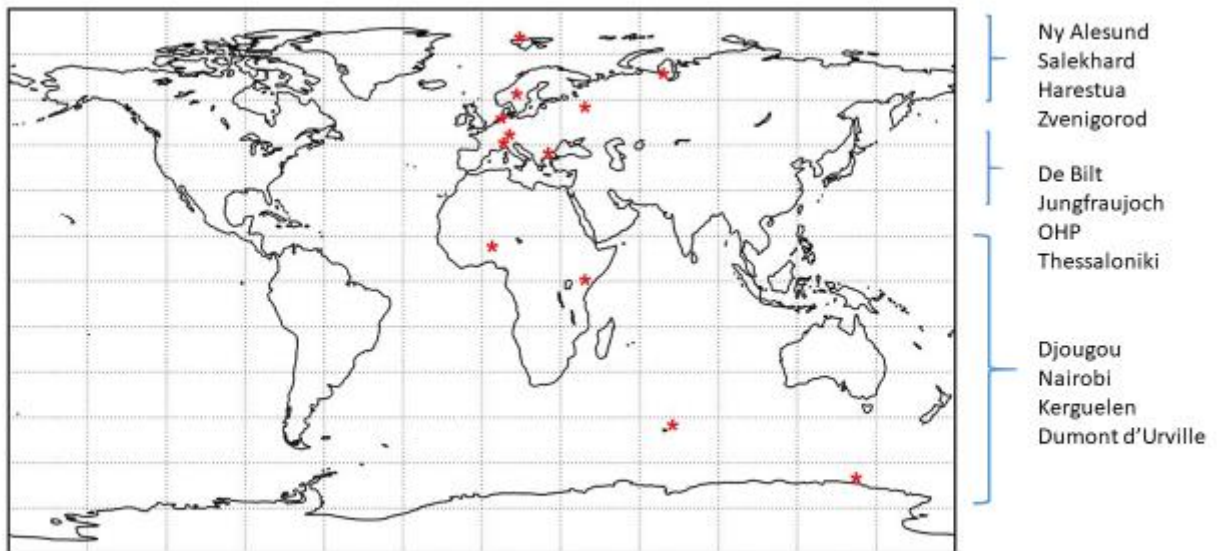
Figure D.4 Overpass sites used for the comparison.

We have extracted GOME-2B and GOME-2C BrO columns above each site for the period February 2019-July 2019. We have calculated monthly averages of these BrO VCDs from the two space instruments for the different sites. In addition, we have calculated a climatological mean of SCIAMACHY BrO measurements between 2007 and 2010. Figure D.5 and D.6 present the different BrO VCD datasets.
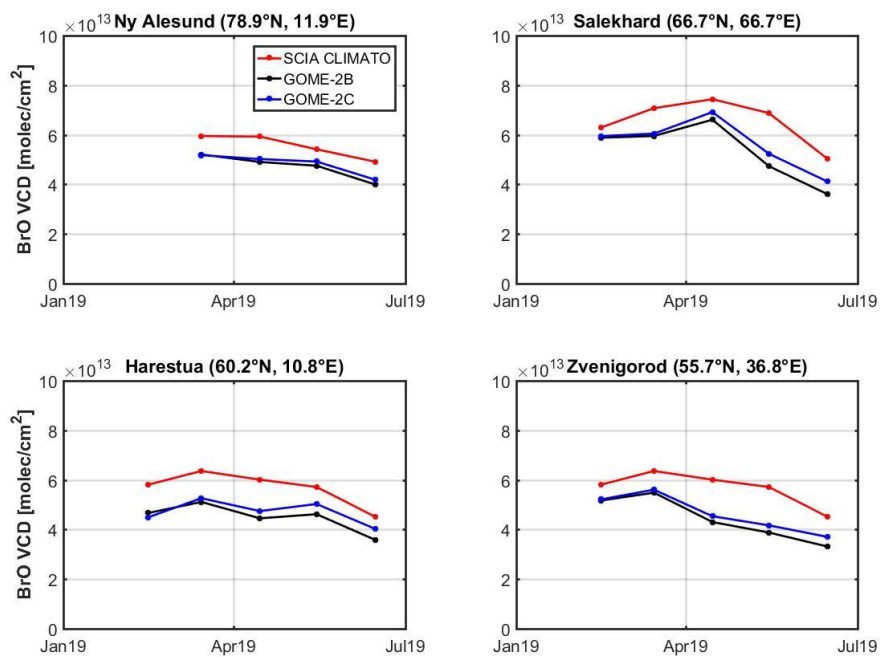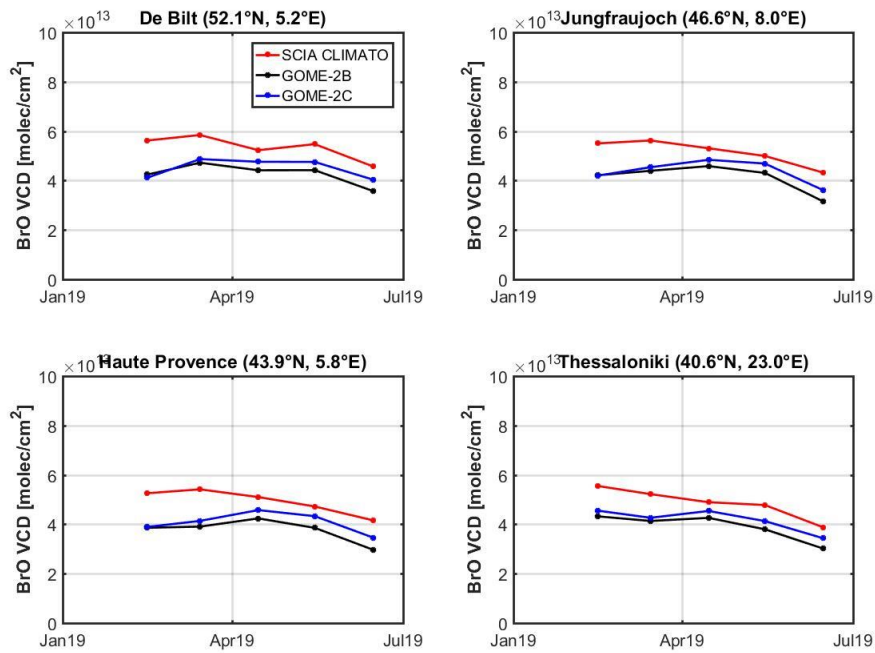
Figure D.5 Comparison of time-series of monthly averaged BrO vertical columns retrieved from GOME-2B and GOME-2C over the February 2019- July 2019 period at the overpass sites of Figure D.4.Also shown is the 2007-2010 mean of SCIAMACHY BrO VCDs.
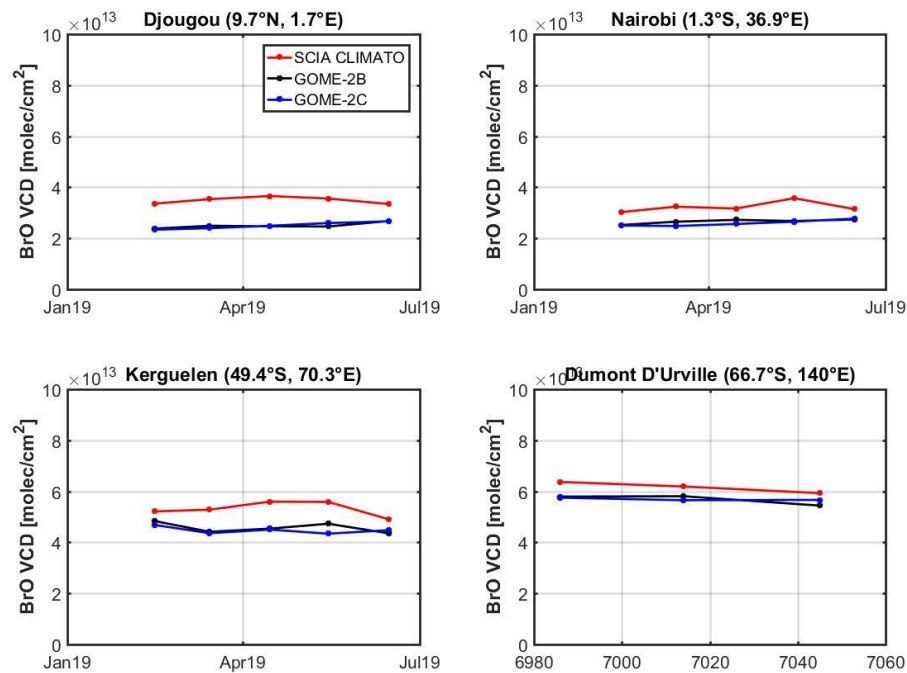
Figure D.5 Continued.

GOME-2B and GOME-2C BrO VCDs show a good agreement at all stations, the relative difference between the two sensors remains within 15%. At all the northern hemisphere sites except Djougou (the most southern site north of the Equator at 9.7°N), GOME-2C is slightly higher than GOME-2B. This is not the case for the four last overpass sites, which are the most southern, for which no clear bias appears between the two GOME-2 datasets.

GOME-2B and GOME-2C shows lower BrO VCDs than the SCIAMACHY climatology. This can be partly explained by the decreasing trend of BrO VCDs observed since 2001 (-0.5%/year, F. Hendrick, personal communication) and by the larger swath of GOME-2 when compared to SCIAMACHY. Larger viewing angles yield larger AMFs when compared to SCIAMACHY. On the other hand, due to the tropospheric BrO content, the true AMF is as overestimated as the viewing angle is large, which may result in a low bias for the GOME-2 BrO VCDs. This effect was already investigated in the previous validation exercise.

Figure D.6 presents, for all the overpass sites, the relative differences between GOME-2C and GOME-2B of all monthly averaged BrO VCDs as a function of the BrO GOME-2B column for the Feb. 2019-Jul. 2019 period. The relative differences between GOME-2C and GOME-2B BrO VCDs are mainly within the optimal accuracy, one point being within in target accuracy.
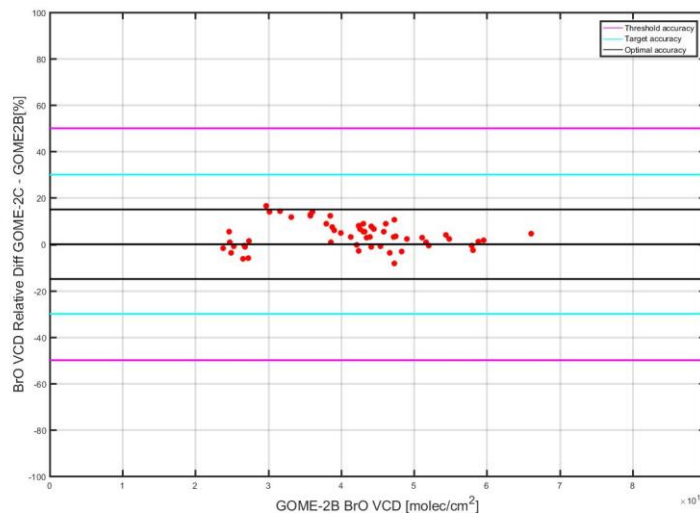
Figure D.6 Relative difference in the monthly averaged BrO VCD (see Figure D.5) between GOME-2C and and GOME-2b (black points) plotted as a function of GOME-2B BrO VCD.

Figure D.7. compares both datasets in a scatter plot. The correlation is 0.97 and the slope is 0.98, with an intercept of 0.19×10^{13} molec.cm^{-2} for GOME-2C with respect to GOME-2B.
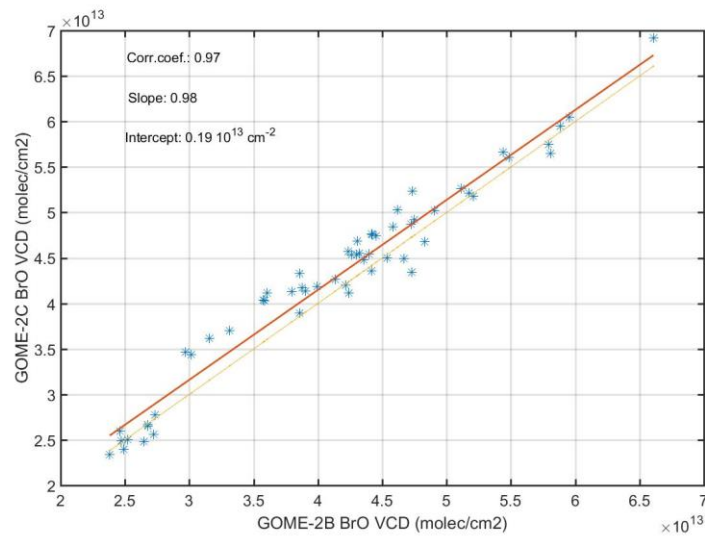
Figure D.7 Relative difference in the monthly averaged BrO VCDs (see Figure D.5) between GOME-2C and and GOME-2B (black points) plotted as a function of GOME-2B BrO VCDs
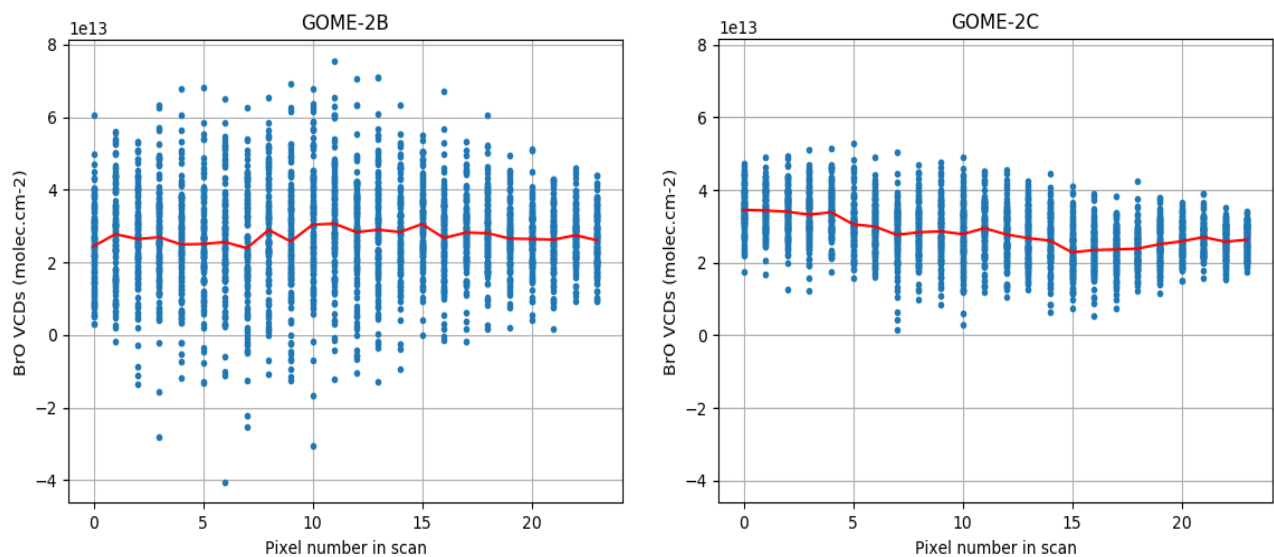
Figure D.8 BrO VCDs from GOME-2B and GOME-2C for the reference dataset presented on Fig. C4.

Figure D.8 finally compares the BrO GOME-2B and GOME-2C VCDs for the reference area and orbits defined in section C.3. The enhancement which is visible in the BrO SCDs for GOME-2C is still visible but less pronounced, with a maximum of 40% on pixel 0 compared to pixel 15. As for the SCDs, the realistic baseline seems to be around pixel 15 when compared to GOME-2B. Such an enhancement is qualitatively consistent with the small positive bias of GOME-2C compared to GOME-2B which is observed for most of the stations in Fig.D.5.

D.3   Comparison against ground-based data

The direct comparison of GOME-2 BrO columns with ground-based correlative sources is under progress. In this report, we focus on a first comparisons with zenith-sky measurements at the Harestua station in Southern Norway.

D.3.1 Comparison with Zenith-sky observations at Harestua

GOME-2B (GDP4.8) and -2C (GDP4.9) total columns of BrO have been compared to ground-based UV-visible zenith-sky measurements at Harestua, Norway (60°N, 11°E) for the January-July 2019 period. Ground-based columns are derived from vertical profiles retrieved by applying an OEM (Optimal Estimation Method)-based profiling technique to zenith-sky measurements at sunrise (Hendrick et al., 2007). The sensitivity of these measurements to the troposphere is increased by using a fixed reference spectrum corresponding to clear-sky noon summer conditions for the spectral analysis. In order to ensure the photochemical matching between satellite and ground-based observations, sunrise ground-based columns have been photochemically converted to the satellite overpass SZAs using a stacked box photochemical model (Hendrick et al., 2007 and 2008). Comparison results (150 km overpasses) are shown in Figures D.8 and D.9 and mean biases and standard deviations are summarized in Table D.1. The agreement between GOME-2C and ground-based observations is good with mean biases of -12 ± 10 %. The corresponding bias values for GOME-2B are -15 ± 11 %. These different biases are consistent with the findings of Section D.2, where GOME-2C appears slightly above GOME-2B for most of the stations. Both values are thus within the optimal accuracy of 15 %. Note that for both spaceborne instruments, the difference with the ground-based measurements is larger in winter. This may be due to the AMF used in the satellite products. We may check this hypothesis using a more accurate satellite AMFs calculated from the ground-based measured profiles. This will be done when more data will be available.

	GOME-2B (stratospheric AMF)	GOME-2C (stratospheric AMF)
Mean bias with ground-based observations (%)	-15 ± 11	-12 ± 10

Table D.1: mean biases between GOME-2 (B and C) and ground-based BrO observations at Harestua (60°N, 11°E) for the January-July 2019 period.
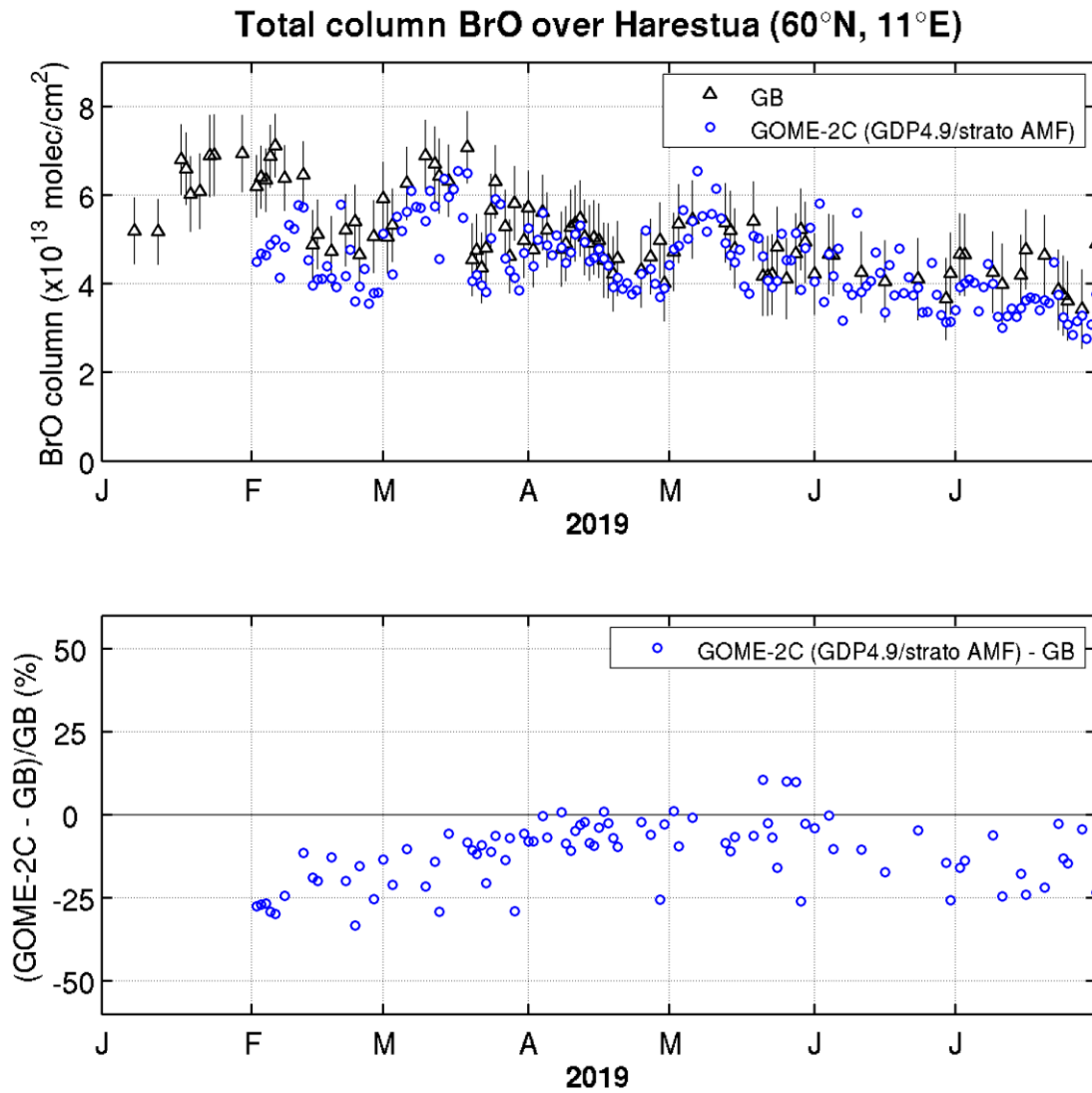
Figure D.8: Comparison between GOME-2C GDP-4.9 and ground-based total BrO columns at Harestua (60°N, 11°E). The relative differences appear in the lower plot.

Total column BrO over Harestua (60°N, 11°E)
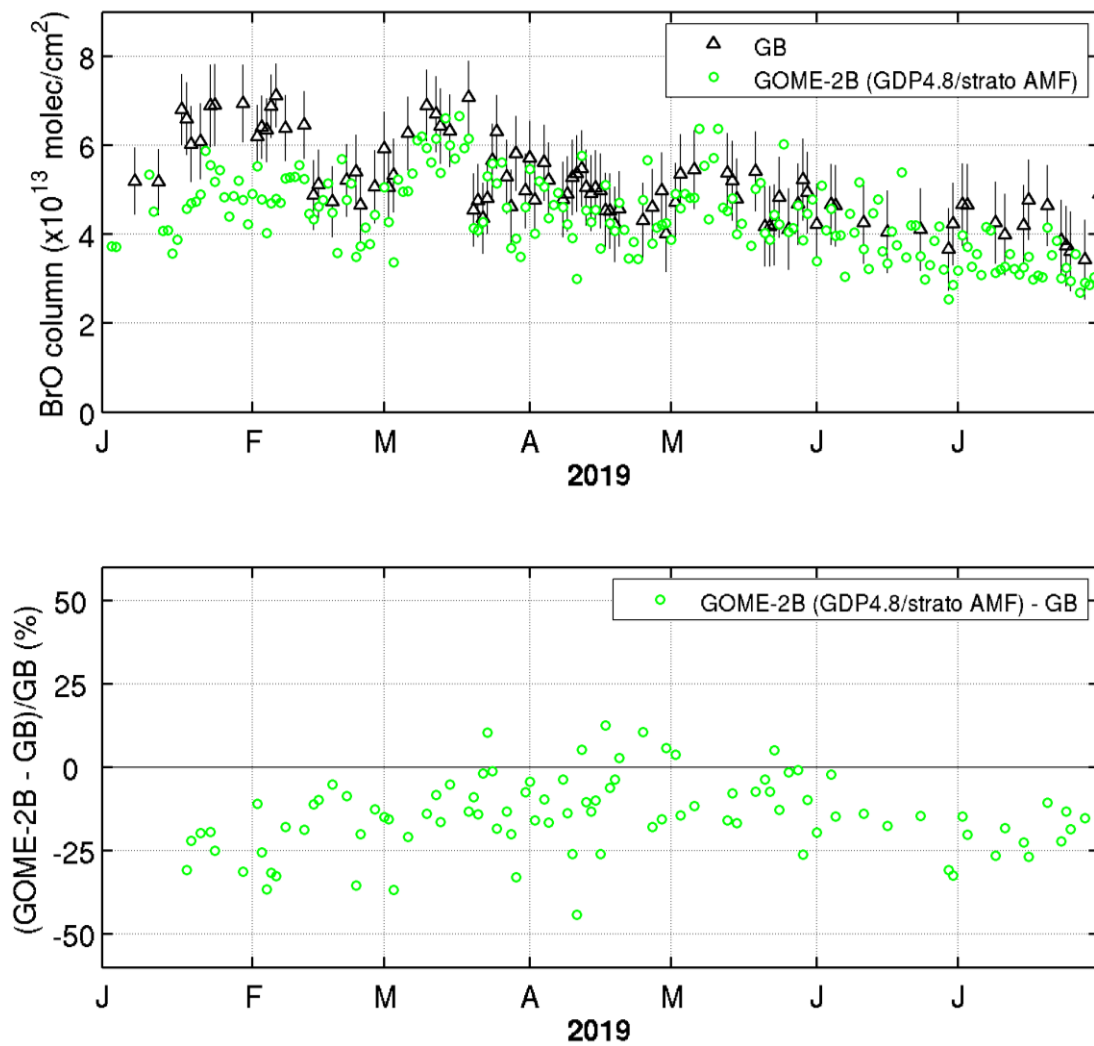
Figure D.9: Similar as Figure D.8 but for GOME-2B GDP-4.8.

E. CONCLUSION AND PERSPECTIVES

This document reports on the validation of AC-SAF GOME-2C BrO column data products retrieved at DLR with versions 4.9 of the GOME Data Processor (GDP), using level-1B-R1 data based on level-0-to-1B processor version 6.3.

We have evaluated GOME-2C BrO vertical columns using (1) scientific retrievals based on the BIRA-IASB tools and (2) comparisons with correlative data sets from SCIAMACHY, GOME-2A, GOME-2B and from ground-based zenith-sky measurements.

For verification purpose, we compared the GDOAS and GDP 4.9 retrievals and a reasonably good agreement was found, confirming the reliability of the GDP for BrO slant column fitting. However, we detected an angular dependence in the BrO SCDs, with enhanced values on the edge of the swath. This dependence corresponds to an inverse pattern observed in the GOME-2C H_2CO product. Such a cross talk between the two species is understood from their spectral interference. On the other hand, the origin of the angular dependence itself is not understood at the time of writing this report. It may be linked to a polarization sensitivity of the GOME-2C instrument but this deserves further investigation.

Users requiring the highest BrO column accuracy for a given overpass should only use the G2-C pixels 7-17. The positive bias we observed in the reference area between the BrO SCDs at the center and the edge of the swath (80%) is reduced in the BrO VCDs due to the AMF dependency on the viewing zenithal angle, and it is further smoothed as they are averaged. Yet the users should consider a possible overestimation of the G2C BrO VCDs of a few percent in the monthly-averaged G2C BrO VCDs.

The difference between GOME-2C and GOME-2B data show a small positive bias for the northern overpass sites in the investigated period (Feb-Jul 2019). This is consistent with the aforementioned angular dependence. However, in a majority of cases (>90% of the time), the GOME-2C GDP 4.9 total BrO column product agrees within 15% with GOME-2B. Additional comparisons using the latest version of available ground-based DOAS measurements at the NDACC station of Harestua (Norway) further consolidate the findings of the GOME-2 B and C comparison, with mean bias within the optimal accuracy (15%) as stated in the ACSAF Service Specification Document.

Based on the validation with ground-based measurements and the comparisons with correlative satellite data, we conclude that the current GOME-2B GDP 4.9 BrO column product (based on the limited period Feb 2019-Jul. 2019) fulfill the user requirements in terms of accuracy (target accuracy, virtually all the time ; optimal accuracy, in a majority of cases).

Further validation of the BrO total VCD should include ground-based columns observations at other sites than Harestua. Moreover, in a later stage, retrievals of tropospheric BrO columns based on the total BrO slant columns should be undertaken.

F. REFERENCES

F.1. Applicable documents

[ATBD] Algorithm Theoretical Basis Document - GOME-2 Total Column Products of Ozone, NO_2, BrO, HCHO, SO_2, H_2O, OClO, and Cloud Properties (GDP 4.8 for AC SAF OTO and NTO), Valks, P., Loyola D., Hao N., Hedelt, P., Slijkhuis S., Gross, M., Gimeno Garcia, S., Lus, R., 2017, https://acsaf.org/docs/atbd/Algorithm_Theoretical_Basis_Document_NTO_OTO_DR_GDP48_Jun _2017.pdf

[PUM]   Valks, P., et al., (2017), Product User Manual for GOME Total Column Products of Ozone, NO2, BrO, HCHO, SO2, H2O, OClO and Cloud Properties, GDP 4.8, SAF/AC/DLR/PUM/01, Iss. 3/A, Rev. 2, June, 2017, https://acsaf.org/docs/pum/Product_User_Manual_NTO_OTO_DR_GDP48_Jun_2017.pdf

F.2. Reference documents

F.2.1 Peer-reviewed articles

Bogumil, K., Orphal, J., Homann, T., Voigt, S., Spietz, P., Fleischmann, O.C., Vogel, A., Hartmann, M., Bovensmann, H., Frerik, J., and Burrows, J. P.: Measurements of molecular absorption spectra with the SCIAMACHY Pre-Flight Model: Instrument characterization and reference spectra for atmospheric remote sensing in the 230-2380 nm region, J. Photochem. Photobiol. A, 157, 167-184, 2003.

Brion, J., Chakir, A., Charbonnier, J., Daumont, D., Parisse, C. and Malicet, J., Absorption spectra measurements for the ozone molecule in the 350-830 nm region, J. Atmos. Chem., 30, 291-299, 1998.

Brion, J., Chakir, A., Daumont, D. and Malicet, J., High-resolution laboratory absorption cross section of O3. Temperature effect, Chem. Phys. Lett., 213 (5-6), 610-512, 1993.

Fleischmann, O. C., Hartmann, M., Burrows J. P., and Orphal, J.: New ultraviolet absorption cross-sections of BrO at atmospheric temperatures measured by time-windowing Fourier transform spectroscopy, J. Photochem. Photobiol. A, 168, 117–132 , 2004.

Hendrick, F., M. Van Roozendael, M. P. Chipperfield, M. Dorf, F. Goutail, X. Yang, C. Fayt, C. Hermans, K. Pfeilsticker, J.-P. Pommereau, J. A. Pyle, N. Theys, and M. De Mazière, Retrieval of stratospheric and tropospheric BrO profiles and columns using ground-based zenith-sky DOAS observations at Harestua, 60°N, Atmospheric Chemistry and Physics, 7, 4869-4885, 2007

Hendrick, F., Johnston, P.V., De Mazière, M., Fayt, C., Hermans, C., Kreher, K., Theys, N., and Van Roozendael, M.: One-decade trend analysis of stratospheric BrO over Harestua (60°N) and Lauder (45°S) reveals a decline, Geophys. Res. Lett., 35, L14801, doi:10.1029/2008GL034154, 2008.

Hendrick, F., A. Rozanov, P. V. Johnston, H. Bovensmann, M. De Mazière, C. Fayt, C. Hermans, K. Kreher, W. Lotz, B.-M. Sinnhuber, N. Theys, A. Thomas, J. P. Burrows, and M. Van Roozendael, Multi-year comparison of stratospheric BrO vertical profiles retrieved from SCIAMACHY limb and ground-based UV-visible measurements, Atmospheric Measurement Techniques, 1, 273-285, 2009

Meller, R., and Moortgat, G. K.: Temperature dependence of the absorption cross-section of HCHO between 223 and 323K in the wavelength range 225-375 nm, J. Geophys. Res., 105(D6), 7089-7102, doi: 10.1029/1999JD901074, 2000.

Pinardi, G., Van Roozendael, M., Abuhassan, N., Adams, C., Cede, A., Clémer, K., Fayt, C., Frieß, U., Gil, M., Herman, J., Hermans, C., Hendrick, F., Irie, H., Merlaud, A., Navarro Comas, M., Peters, E., Piters, A. J. M., Puentedura, O., Richter, A., Schönhardt, A., Shaiganfar, R., Spinei, E., Strong, K., Takashima, H., Vrekoussis, M., Wagner, T., Wittrock, F., and Yilmaz, S.: MAX-DOAS formaldehyde slant column

measurements during CINDI: intercomparison and analysis improvement, Atmos. Meas. Tech., 6, 167–185, https://doi.org/10.5194/amt-6-167-2013, 2013

Richter, A., Wittrock, F., Ladstätter-Weissenmayer, A., and Burrows, J. P.: GOME measurements of stratospheric and tropospheric BrO, Adv. Space Res., 29, 1667-1672, 2002.

Puķīte, J., Kühl, S., Deutschmann, T., Platt, U., and Wagner, T.: Extending differential optical absorption spectroscopy for limb measurements in the UV, Atmos. Meas. Tech., 3, 631-653, 2010.

Theys, N., Van Roozendael, M., Errera, Q., Hendrick, F., Daerden, F., Chabrillat, S., Dorf, M., Pfeilsticker, K., Rozanov, A., Lotz, W., Burrows, J. P., Lambert, J.-C., Goutail, F., Roscoe, H. K., and De Mazière, M.: A global stratospheric bromine monoxide climatology based on the BASCOE chemical transport model, Atmos. Chem. Phys., 9, 831-848, 2009.

Theys, N., Van Roozendael, M., Hendrick, F., Yang, X., De Smedt, I., Richter, A., Begoin, M., Errera, Q., Johnston, P. V., Kreher, K., and De Mazière, M.: Global observations of tropospheric BrO columns using GOME-2 satellite data, Atmos. Chem. Phys., 11, 1791-1811, 2011.

F.2.2 Technical notes

O3-SAF Validation Report, Offline total bromine oxide SAF/O3M/BIRA/VR/BRO/091 17 Nov 2009, http://o3msaf.fmi.fi/docs/vr/Validation_Report_OTO_BRO_Nov_2009.pdf.

O3M-SAF, Validation report of GOME-2 offline and reprocessed GDP 4.8BrO total column data for MetOp-A and B SAF/O3M/BIRA/VR/BRO/, 9 Dec 2015 https://acsaf.org/docs/vr/Validation_Report_OTO_DR_BrO_GDP48_Dec_2015.pdf

AC-SAF, Operations Report, Reporting period Jan-Jun 2019 SAF/AC/FMI/OPS/RP/001, 10 Sept. 2019, https://acsaf.org/docs/or/AC_SAF_Operations_Report_1-2019.pdf

AC-SAF, ORR Validation report, SAF/AC/IASB/VR/HCHO, February 2019 – July 2019, 25 Nov. 2019